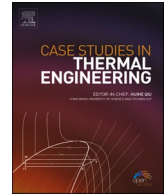




ELSEVIER

Contents lists available at [ScienceDirect](https://www.sciencedirect.com)

Case Studies in Thermal Engineering

journal homepage: www.elsevier.com/locate/csie

Optimizing air inlet designs for enhanced natural ventilation in indoor substations: A numerical modelling and CFD simulation study

Haomai Zhang^a, Ling Wang^a, Peng Yang^{a,**}, Yingwen Liu^{a,*}, Chao Zhu^b,
Lv Wang^b, Hua Zhong^c

^a Key Laboratory of Thermo-Fluid Science and Engineering of MOE, School of Energy and Power Engineering, Xi'an Jiaotong University, Xi'an, 710049, China

^b State Grid Shaanxi Electric Power Research Institute, Xi'an, 710000, China

^c London South Bank University, SE1 0AA, UK

ARTICLE INFO

Keywords:

Computational fluid dynamics
Numerical simulation
Indoor substation cooling
Natural ventilation
Heat dissipation
Air inlet design

ABSTRACT

This paper investigates the ventilation and heat dissipation performance of a 110 kV indoor substation under natural ventilation conditions using computational fluid dynamics (CFD). The objectives are to evaluate the influences of air inlet design parameters including location and size, and transformer load, on the airflow distribution, temperature field, and cooling efficiency. The study finds that staggered opposite inlets optimize cooling uniformity without airflow attenuation. Compared to a single inlet, the maximum transformer temperature is reduced by 1.3 °C and energy utilization increases by 9.1 % with staggered inlets. Increasing the inlet length ratio initially improves cooling until an optimal point (The length ratio is 1.10), while reducing the inlet height ratio decreases airflow and efficiency. With load increasing, the intake airflow rises but at a reduced rate, and the temperature difference can exceed 15 °C under high loads. In summary, optimizing inlet design enhances natural ventilation performance in indoor substations, but limitations exist at high loads, indicating supplemental mechanical ventilation may be required.

1. Introduction

With rising electricity demand from residential and commercial sectors, indoor substations are increasingly being constructed in urban areas due to land constraints. However, the heat dissipated from transformers and other equipment in these indoor substations can lead to excessive temperature build-up. Natural ventilation systems are often preferred for indoor substations because of lower operating costs compared to mechanical ventilation. Additionally, the lack of fans results in lower noise, making natural ventilation more suitable for indoor sites. Therefore, there is a critical need to optimize the natural ventilation configurations for indoor substations to maximize heat removal while minimizing land usage.

The indoor substation with natural ventilation relies on the temperature difference between indoor and outdoor for ventilation. The flow and heat transfer in the main transformer room are complicated, and the physical property parameters of the air change with the

* Corresponding author.

** Corresponding author.

E-mail addresses: yp2019@mail.xjtu.edu.cn (P. Yang), ywliu@mail.xjtu.edu.cn (Y. Liu).

<https://doi.org/10.1016/j.csie.2024.104408>

Received 27 December 2023; Received in revised form 11 April 2024; Accepted 16 April 2024

Available online 7 May 2024

2214-157X/© 2024 The Authors. Published by Elsevier Ltd. This is an open access article under the CC BY-NC license (<http://creativecommons.org/licenses/by-nc/4.0/>).

temperature, so this kind of problem is a complicated nonlinear problem. They are often solved by numerical method. Finite element method [1–3] and finite volume method are two commonly used methods to obtain numerical solutions. CFD software based on these two methods came into being. In the research of indoor substations, due to its large space, it is difficult to use experimental methods to conduct detailed research on its internal flow and temperature field, and most of the research uses CFD software for numerical simulation. Xie et al. [4] analysed the influences of ventilation quantity, location, and size of the inlet and outlet on ventilation and heat dissipation. Liu et al. [5] developed a new ventilation optimisation method based on the variational method to solve ventilation and heat transfer problems. Kanaan M and Chahine K [6] studied 7 different ventilation schemes of a main transformer chamber with multi-zone transformers. Xu and Zou [7] proposed a fast computational fluid dynamics (FFD) method to establish a substation model which can effectively represent the flow and heat dissipation characteristics of the substation. Liu et al. [8] studied the influence of the installation positions of fans on the heat dissipation effect of the transformer. Yang et al. [9] conducted simulation research on six different ventilation schemes of the main transformer chamber. Cheng et al. [10] analysed the influence of the box-in structure on the temperature rise of the transformer and its surrounding environment under different ambient wind speeds. Wei et al. [11] studied the influence of critical natural ventilation temperature, mechanical ventilation rate, and size and location of the inlet on split-type indoor transformers. Wei et al. [12] proposed a simulation device suitable for the experiment of a split cooling device. Ramos et al. [13] conducted a numerical simulation of natural ventilation in two underground substations and obtained the functional relationship between air flow rate and transformer heat dissipation. A. Bidarmaghz et al. [14] proposed a cooling method using heat pump to absorb heat in substation and release it into tunnel through heat exchanger. Wang et al. [15] combined solar photovoltaic power generation system, air source heat pump system and natural ventilation to achieve energy saving and carbon reduction in the substation.

Some scholars have studied ventilation and heat dissipation in other buildings. S. Wiriyasart and P. Naphon [16] analysed the effects of unilateral and central air inlets on air and temperature distribution in a multi-heat source workshop. Zheng et al. [17] studied the performance of an air conditioning system with two air supply modes for a simplified office chamber. S.-J. Mei et al. [18] found that adding auxiliary mechanical ventilation on the basis of natural ventilation could reduce air temperature and improve air exchange efficiency. Ang et al. [19] implemented natural ventilation in the classroom and improved natural ventilation performance by optimizing the angle of shutters and introducing wind traps. Yue et al. [20] investigated the effects of different solar radiation intensities, heat flow density and location of indoor heat sources and wind speed on the natural ventilation performance of solar chimneys. Yang [21] studied the influence of heat source height and opening area on natural ventilation. Tao et al. [22] studied the ventilation performance of a naturally ventilated double-skin. Chen et al. [23] conducted an experimental study on the influence of natural ventilation on residential thermal environment and thermal comfort in rural areas. Tantasavasdi et al. [24] aims to explore the efficiency of natural ventilation in the bedrooms of typical two-storeyed row houses with cross ventilation. Li et al. [25] used a combination of natural ventilation, external shading and cool roof to improve the indoor thermal environment. The problems of natural convection and radiation heat transfer are also indispensable in the study of substation. The problems of natural convection and radiation heat transfer in confined space have been studied. R. Hidki et al. [26] numerically studied the mixed convection coupled with surface radiation in a ventilated horizontal channel. M. Foruzan Nia et al. [27] investigated the problems of natural convection and radiative heat transfer in electronic devices and used the DOM method to solve the radiative transfer equation. R. Hidki et al. [28] focused on the cooling by natural convection and surface radiation of two electronic components generating two different and uniform volumetric powers.

Natural ventilated buildings (including substations) are ventilated by either indoor or outdoor wind or thermal pressure. Ventilation volume is one of the key factors affecting buildings with natural ventilation. Changing the inlet area is a common method for changing the intake air volume. While ventilation performance in indoor substations has been studied, there remains a lack of research on how the design of air inlets and load rate affects parameters like airflow rate, temperature distribution, and heat dissipation performance under natural ventilation conditions specifically. This study addresses this gap by modelling an indoor substation with

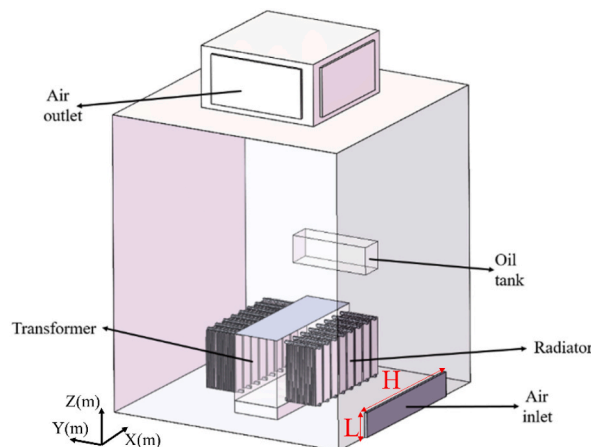


Fig. 1. Model of the main transformer chamber.

different inlet configurations and quantitatively evaluating the resulting heat dissipation performance through velocity profiles, temperature measurements, and energy utilization coefficients. This research aims to numerically evaluate the efficacy of different air inlet designs and transformer operating loads on the ventilation and heat dissipation performance through STAR CCM + software based on finite volume method. The findings empower infrastructure planners and substation designers to create tailored, high-performance ventilation schemes that maximize reliability. Strategic inlet configurations are vital to extract rising heat loads, especially as electricity demands grow.

2. Physical model

The model of an indoor substation was constructed according to the common type of natural ventilation. The model is simplified as follows: (1) the main transformer is simplified into a cuboid of the same size; (2) the radiator is simplified into cuboid slices. Fig. 1 shows the original model of the main transformer chamber consisting of the main transformer, radiators, and oil tank. The transformer is located in the middle of the chamber. The height between the bottom of the transformer and the ground of the chamber is 0.48 m. Sixteen sets of radiators are on both sides of the main transformer. The width of the radiators and transformer is 4.95 m. Table 1 shows the sizes of these components. For convenient description, the ventilation scheme represented by this model is called Scheme 1.

3. The numerical method

The following assumptions are adopted in this paper.

- (1) The fluid flow in this study is characterized as three-dimension model, steady state and incompressible flow.
- (2) Only natural ventilation driven by indoor and outdoor temperature differences is considered. The influence of external environmental changes (wind speed and direction) is ignored.
- (3) The change of air density due to the change of temperature adopts the Boussinesq hypothesis.

3.1. Governing equations

A three-dimensional model is used to analyse the temperature and flow fields in the main transformer chamber. Although the process of airflow and heat transfer in the chamber is complicated, it satisfies the continuity [29], momentum and energy equations [13]. These governing equations are shown in equations (1)–(3):

$$\frac{\partial(\rho \vec{u}_i)}{\partial x_i} = 0 \quad (1)$$

$$\frac{\partial}{\partial x_j} (\rho \vec{u}_i \vec{u}_j) = -\frac{\partial p}{\partial x_i} + \frac{\partial}{\partial x_j} \left[(\mu + \mu_T) \left(\frac{\partial \vec{u}_i}{\partial x_j} + \frac{\partial \vec{u}_j}{\partial x_i} \right) - \frac{2}{3} \rho \kappa \delta_{ij} \right] - g_i (\rho - \rho_0) \quad (2)$$

$$\frac{\partial}{\partial x_i} (\rho c_p T \vec{u}_i) = \frac{\partial}{\partial x_i} \left[(\lambda + \lambda_T) \frac{\partial T}{\partial x_i} \right] + \nabla \cdot \vec{q}_r \quad (3)$$

where ρ is density, $\text{kg}\cdot\text{m}^{-3}$; \vec{u}_i is velocity vector, $\text{m}\cdot\text{s}^{-1}$; x_i is directional component, m; p is pressure, Pa; μ is dynamic molecular viscosity, $\text{m}^2\cdot\text{s}^{-1}$; μ_T is turbulent eddy viscosity, $\text{m}^2\cdot\text{s}^{-1}$; g_i is acceleration of gravity, $\text{m}\cdot\text{s}^{-2}$; c_p is specific heat capacity, $\text{J}\cdot\text{kg}^{-1}\cdot\text{K}^{-1}$; λ is thermal molecular conductivity, $\text{W}\cdot\text{m}^{-1}\cdot\text{K}^{-1}$; λ_T is turbulent thermal conductivity, $\text{W}\cdot\text{m}^{-1}\cdot\text{K}^{-1}$; T is temperature, K. $\nabla \cdot \vec{q}_r$ is the radiation source term. Since the gas medium participates in radiation heat transfer, its volumetric effect is considered in the conservation of energy as a source term [26]. The expression of the radiation source term is as follows [26]:

$$\nabla \cdot \vec{q}_r = \sigma_a \left(4\pi I_b(\vec{r}) - \int_{4\pi} I(\vec{r}, \vec{s}) d\Omega \right) \quad (4)$$

where σ_a is the absorption coefficient, and I_b is the black body intensity, $\text{W}\cdot\text{m}^{-3}$. $I(\vec{r}, \vec{s})$ is the radiation intensity at the position \vec{r} and in direction \vec{s} .

Because the steady-state problem is studied in this paper, the time term is not considered in the above governing equations. When studying natural ventilation, the density change caused by temperature change cannot be ignored; therefore, the buoyancy lift term is added to the right side of the momentum equation (Equation (2)). g_i is the acceleration of gravity in some direction. ρ_0 is the reference

Table 1
Size of major components in the main transformer chamber.

Name	Size
Main transformer chamber(x × y × z)	10 m × 10 m × 12 m
Main transformer(x × y × z)	5.5 m × 1.9 m × 2.3 m
Radiator(x × y × z)	0.52 m × 2 m × 0.01 m
Oil tank(x × y × z)	3.24 m × 0.95 m × 1.1 m
Air nlet(x × z)	6 m × 1 m

temperature. In the simulation process, to simplify the calculation, the Boussinesq hypothesis is often used.

In this paper, the turbulence problem of airflow in the main transformer chamber is solved by the Realizable k - ε model. The governing equations of turbulent kinetic energy k and dissipation rate ε are shown in equations (5) and (6) [14]. Equation (7) further defines factor μ_T of the previous equations.

$$\rho \vec{u}_i \frac{\partial \varepsilon}{\partial x_j} = \frac{\partial}{\partial x_j} \left[\left(\mu + \frac{\mu_T}{\sigma_k} \right) \frac{\partial \varepsilon}{\partial x_j} \right] + \mu_T \left(\frac{\partial \vec{u}_i}{\partial x_j} + \frac{\partial \vec{u}_j}{\partial x_i} \right) \frac{\partial \vec{u}_i}{\partial x_j} - \rho \varepsilon \quad (5)$$

$$\rho \vec{u}_i \frac{\partial k}{\partial x_j} = \frac{\partial}{\partial x_j} \left[\left(\mu + \frac{\mu_T}{\sigma_k} \right) \frac{\partial k}{\partial x_j} \right] + c_1 \mu_T \frac{\varepsilon}{k} \left(\left(\frac{\partial \vec{u}_i}{\partial x_j} + \frac{\partial \vec{u}_j}{\partial x_i} \right) \frac{\partial \vec{u}_i}{\partial x_j} \right) - c_2 \rho \frac{\varepsilon^2}{k} \quad (6)$$

where:

$$\mu_T = \rho c_\mu \frac{k^2}{\varepsilon} \quad (7)$$

where μ is dynamic molecular viscosity, $\text{m}^2 \cdot \text{s}^{-1}$; μ_T is turbulent eddy viscosity, $\text{m}^2 \cdot \text{s}^{-1}$. The values of the model constants c_1 , c_2 , c_μ , σ_k and σ_ε are derived from basic turbulence experiments and have the following default values: c_1 is 1.44; c_2 is 1.92; c_μ is 0.09; σ_k is 1.0; σ_ε is 1.3 [30,31].

In this paper, considering the radiation between the transformer, radiators, and wall, the discrete coordinate method (DOM) is used to solve the radiation transfer equation in STAR CCM + [32]. The radiation transfer equation (RTE) is as follows:

$$\frac{dI_\lambda}{ds} = -\beta_\lambda I_\lambda + k_{a\lambda} I_{b\lambda} + \frac{k_{s\lambda}}{4\pi} \int_{4\pi} I_\lambda \Omega d\Omega + k_{pa\lambda} I_{pa\lambda} + \frac{k_{ps\lambda}}{4\pi} \int_{4\pi} I_\lambda \Omega d\Omega \quad (8)$$

where I_λ is radiation intensity at wavelength λ , $\text{W} \cdot \text{m}^{-3}$; $I_{b\lambda}$ is blackbody intensity at wavelength λ , $\text{W} \cdot \text{m}^{-3}$; s is the distance in the direction, m ; $k_{a\lambda}$ and $k_{s\lambda}$ are absorption coefficient and scattering coefficient; $k_{pa\lambda}$ and $k_{ps\lambda}$ are particle absorption coefficient and particle scattering coefficient, respectively. Ω is the solid angle, sr .

3.2. Boundary conditions

The acceleration of gravity in the z direction is $-9.81 \text{ m} \cdot \text{s}^{-2}$. The thermophysical properties of air at 30°C are shown in Table 2. The material of the main transformer and radiator is aluminium. The physical properties of aluminium are shown in Table 3. The main transformer model selects the 110 kV three-phase on-load oil-immersed self-cooling power transformer, which is the most widely used at present. Detailed parameters are shown in Table 4. In the process of transformer operation, the transformer is affected by no-load loss and load loss and generates heat [8]. The calculation formula for the heating power is as follows:

$$Q = P_0 + \beta^2 P_k \quad (9)$$

where Q is heating power, kW ; P_0 is no-load loss, kW ; β is load rate, and P_k is load-loss, kW .

The boundary conditions are as follows:

- (1) For natural ventilation, the air inlet adopts pressure inlet and the gauge pressure is set to 0 Pa. The air outlet adopts pressure outlet [33–35]. The outlet backflow temperature is 30°C .
- (2) The upper surface of the main transformer is set to a fixed heat flux boundary. The value is $12759.51 \text{ W} \cdot \text{m}^{-2}$.
- (3) The environment temperature is 30°C .
- (4) The interfaces between the solid and fluid domains are set as the coupling surface, and the wall of the main transformer chamber is adiabatic.

3.3. Grid independence

To reduce the number of grids and improve computing efficiency, the cutting body mesh model is selected when the mesh is divided, and the radiator area grid is locally encrypted. Fig. 2 shows that the maximum temperature of the main transformer varies with the number of grids. With the gradual increase in the number of grids, the maximum temperature of the main transformer first increases and then tends to stabilise. Therefore, a grid of 3.8 million is used to conduct the following simulation calculations.

Table 2
Thermophysical properties of air at 30°C .

Physical property parameter	Value
Density	$1.165 \text{ kg} \cdot \text{m}^{-3}$
Thermal conductivity	$0.0267 \text{ W} \cdot \text{m}^{-1} \cdot \text{K}^{-1}$
Specific heat capacity	$1005 \text{ J} \cdot \text{kg}^{-1} \cdot \text{K}^{-1}$
Dynamic viscosity	$1.86 \times 10^{-5} \text{ kg} \cdot \text{m}^{-1} \cdot \text{s}^{-1}$
Coefficient of thermal expansion	$3.3 \times 10^{-3} \text{ K}^{-1}$

Table 3
Physical properties of aluminium.

Physical property parameter	Value
Density	2702 kg·m ⁻³
Thermal conductivity	237 W·m ⁻¹ ·K ⁻¹
Specific heat capacity	903 J·kg ⁻¹ ·K ⁻¹

Table 4
Parameters of the main transformer.

Parameter	Value
Rated capacity	50000 kVA
Rated voltage	(110 ± 8 × 1.25 %)/10.5 kV
Rated current	262.432 kA
No-load loss	24.85 kW
Load loss	180.94 kW
Cooling mode	ONAN

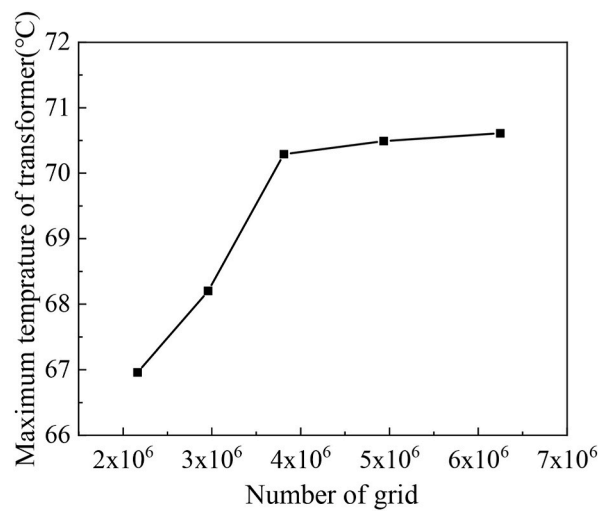


Fig. 2. Grid independence.

4. Model verification

To verify the accuracy of the model, the temperature and air velocity of a 110 kV substation in a field site are evaluated in this paper. The detailed test methods are as follows:

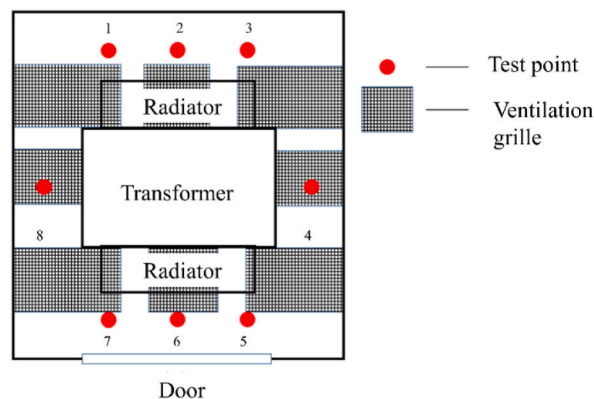


Fig. 3. Location of the test points.

One test point is placed at the inlet in each of the four corners of the main transformer chamber. The test points are located at the geometric centre of the inlet, and the distance from the inlet plane is 0.2 m. Six test points are arranged around the main transformer. When the height of the points is 1 m and 2 m all the test points are 1 m away from the main transformer surface and radiator surface, as shown in Fig. 3. Fig. 4 shows pictures of spot test points.

According to the above numerical method and boundary test data, a numerical simulation of this transformer chamber is conducted. The error analysis between the test and simulation values is shown in Figs. 4 and 5. Figs. 4 and 5 demonstrate that the error of most measuring points can be maintained within the error range of $\pm 15\%$. Therefore, the above calculation method can be applied to this study.

5. Results and discussion

5.1. Analysis of the Baseline Scheme 1

In order to understand the velocity distribution in the main transformer chamber, some cross-sections of the chamber and velocity curve on characteristic lines are selected for analysis, as shown in Fig. 6. From Fig. 6 (a), it can be observed that the velocity distribution at different heights is symmetric about the Y-axis within the range of the inlet height. The indoor and outdoor thermal pressure difference causes chilly air from outside to enter the main transformer chamber. The length of the air inlet is greater than the length of the main transformer, so when the chilly air meets the transformer and is affected by the transformer edge, it leans against the two sides of the transformer, creating a region of low velocity and strong disturbance. This portion of chilly air collects in the area opposite the air inlet and flows into the radiators on the opposite side of the inlet. Due to the small spacing between the radiators, there is a large airflow resistance, resulting in a lower wind speed between the radiators on both sides. After the air is heat exchanged with the radiators, the air temperature rises and the density decreases. The air flows above the main transformer chamber under the action of floating lift. It can be observed from Fig. 6 (b) that the wind speed between the radiators closer to the inlet is higher than that between the radiators on the opposite side of the inlet. In the radiator gap where Line 1 is located, the air velocity is evenly distributed, while in the radiator gap where Line 2 is located, the airflow velocity is higher in the middle and lower on both sides. This indicates the non-uniformity of air volume on both sides.

In order to understand the temperature distribution in the main transformer chamber, some cross-sections of the chamber, temperature curve on characteristic lines and average surface temperature of each group of radiators are selected for analysis, as shown in Fig. 7. From Fig. 7 (a) and (b), a salient thermal stratification exists whereby lower temperatures concentrate below the radiator level, while higher temperatures amass above. Temperatures along the Lines 1 and 2 remain lower than their distal counterparts (Lines 3 and 4). This disparity arises as the radiator area adjoining the air inlet receives greater airflow. Moreover, local temperatures first escalate then moderate above the radiators. The chamber's mean temperatures continually rise with height. For elevations below 4 m, sharp thermal gradients manifest, smoothing out thereafter for $Z \geq 4$ m. At peak heights, the proximal and distal lines convergence towards the mean temperature profile but sustain subtly elevated values. Additionally, Fig. 7 (c) furnishes the mean radiator temperatures across groups 1–8. Proximal radiators exhibit hotter exterior facets amid cooler central regions. This trend owes to significant low-temperature airflow channeling through the midline before heating by thermal exchange. Conversely, groups at the periphery undergo air shunting effects, hampering their cooling efficiency. For distant radiator sets, lateral aspects registrar lower temperatures, whereas central patches peak. Sizeable air disturbances at the lateral edges augment heat transfer to these radiator sections. However, attenuated low-temperature streams reaching the midline compel heightened temperatures here. Furthermore, encompassing temperatures remain higher for the distal radiator groups with their dampened influx volumes. Thus, proximity confers clear cooling advantages with greater air perturbations at the nearby edges forcibly enhancing heat dissipation. Hence, the single-sided inlet configuration induces conspicuous thermal imbalances between the transformer sides.

In summary, according to the velocity and temperature distribution and the curve of changes in local zones, the higher velocity observed at the radiator near the inlet implies greater airflow disturbance in that region, causing enhanced heat transfer and lower temperatures. The trends suggest the single-sided inlet configuration causes imbalanced cooling on both transformer sides. This is not conducive to the heat dissipation of the transformer, and the ventilation performance of the entire main transformer chamber is poor.

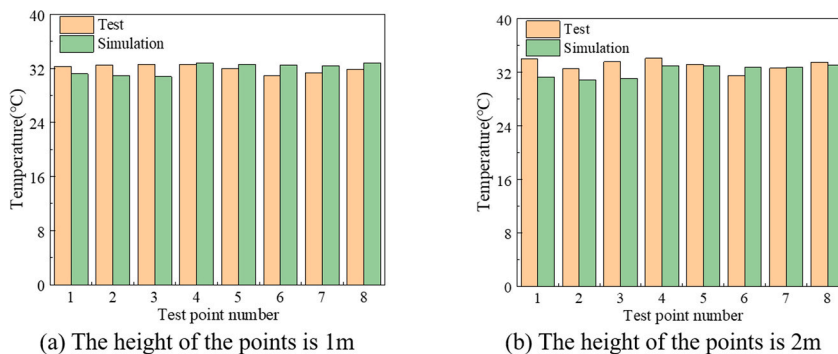


Fig. 4. Temperature error representation of the test and simulation.

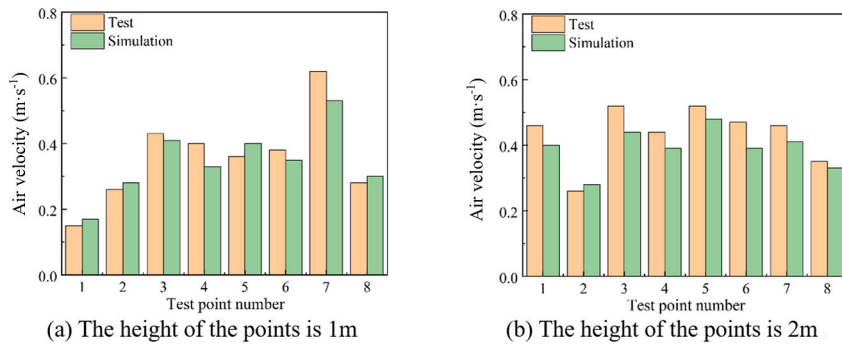


Fig. 5. Air velocity error representation of the test and simulation.

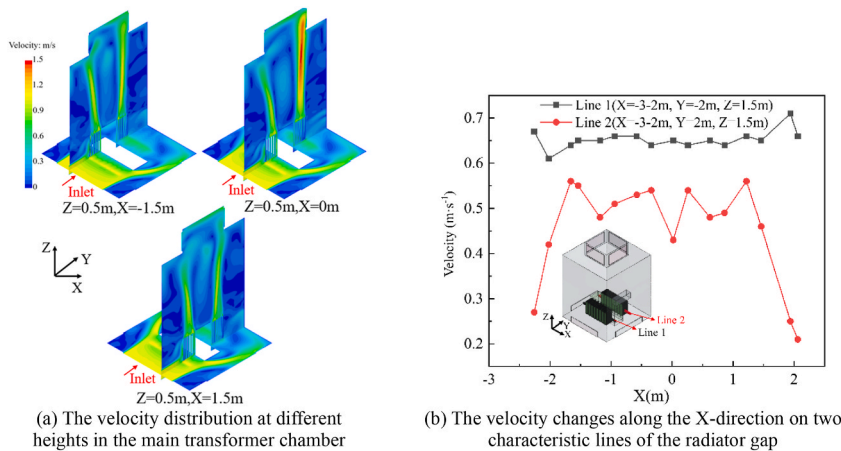


Fig. 6. The velocity distribution in the main transformer chamber.

5.2. Impact of inlet structure parameters

5.2.1. The location of the air inlet affects the temperature field distribution and ventilation

The above section is found that the position of the air inlet has an impact on the distribution of temperature and the flow of air in the main transformer chamber. To further investigate this influence, two different air inlet position schemes were designed based on the relationship between the air inlet and the plane where the radiators are located. The total ventilation area of the inlet was kept constant at 6 m². The details of these two schemes are provided in Table 5, which includes information about the position of the inlet. Numerical simulations were conducted for both schemes to study how the location of the inlet affects the ventilation and heat dissipation characteristics in the main transformer chamber.

Table 6 shows the velocity distribution of different cross-sections in the main transformer chamber under three different air inlet arrangement schemes. As can be seen from Table 6 and in Baseline Scheme 1, as analysed in section 5.1, the area near the inlet has higher wind speed, while the area away from the inlet has lower wind speed. In Scheme 2, the air intake is located at the central bottom of the wall of the main transformer chamber and is perpendicular to the plane where the radiators are located. This arrangement allows outdoor air to flow evenly into the bottom of the radiators on both sides of the transformer. As the air flows through the radiators, it exchanges heat with them, causing its temperature to increase and its density to decrease. Eventually, the air flows above the main transformer chamber. This arrangement causes the air velocity distribution at the bottom of the radiators to gradually contract and the air velocity distribution above the radiators to be inclined. While this arrangement solves the problem of uneven air volume in the radiators on both sides of the transformer, it also leads to a decrease in air speed along the direction of airflow, resulting in uneven cooling of the radiators. In Scheme 3, the air intake is located at the central bottom of the two opposite walls of the main transformer chamber and is perpendicular to the plane where the radiators are located. This arrangement allows outdoor air to flow into the main transformer chamber from the two air intakes simultaneously. Due to the relative flow of the two parts of the air, some of the air impacts the middle of the radiators, causing a small portion of the air to skew to the outside of the radiators. However, this disturbance at the bottom of the radiators enhances the heat exchange between the air and the surface of the radiators. Compared to Baseline Scheme 1 and Scheme 2, this air intake arrangement like Scheme 3 solves the problem of uneven air volume distribution on both sides of the transformer. Additionally, it also solves the problem of air attenuation towards the airflow and ensures the cooling uniformity of the radiators to the greatest extent.

Fig. 8 contains the temperature distribution of cross sections at different inlet locations and average surface temperature of each

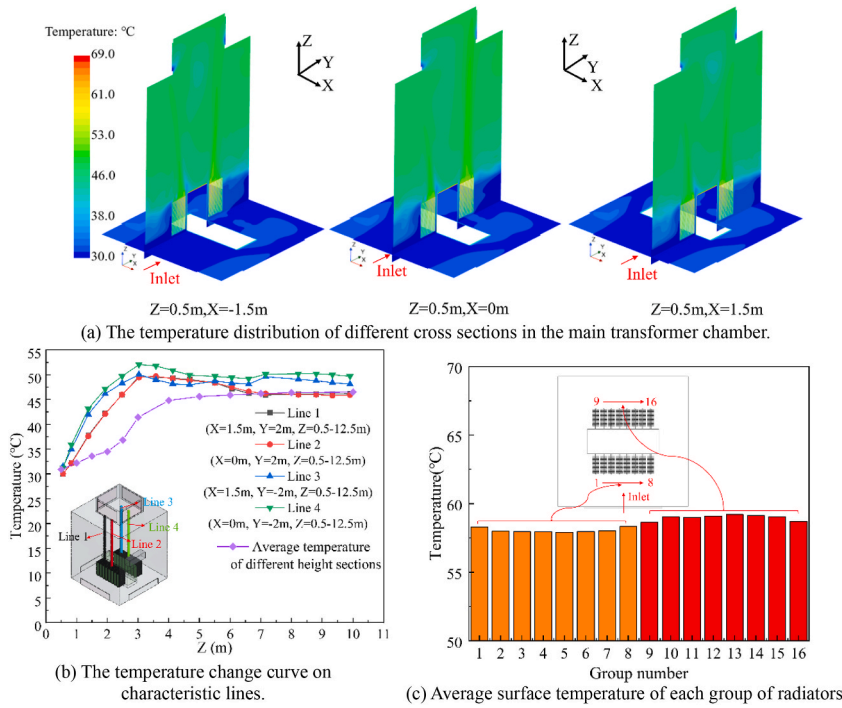


Fig. 7. Temperature distribution in the main transformer chamber.

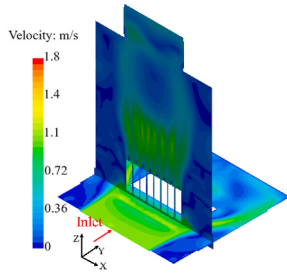
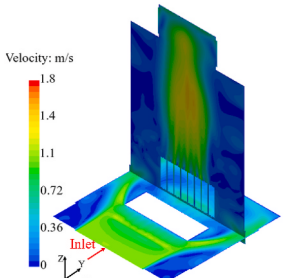
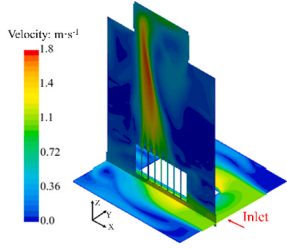
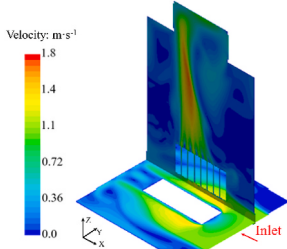
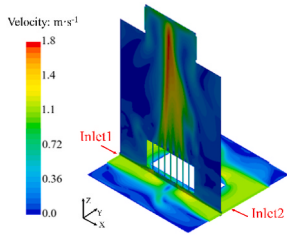
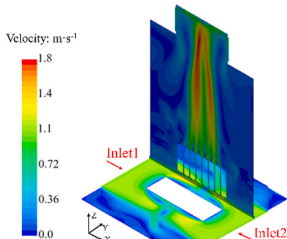
Table 5
Natural air inlet location design schemes.

Scheme	2	3
Picture		
Description	Perpendicular to the radiators, the middle of the bottom of the wall	Perpendicular to the radiators, the middle of the bottom of two opposite walls
Size of inlet ($L \times H \times$ number)	6 m \times 1 m \times 1	6 m \times 0.5 m \times 2

group of radiators at different inlet locations.

As shown in Fig. 8 (a), (b) and (c), the overall temperature distribution trend in the chamber is such that the indoor air temperature increases with an increase in height. From a local perspective, the high-temperature zone is concentrated above the radiators, which are the heat dissipation components in the chamber. Under the condition of natural ventilation, the high-temperature air diffuses in the main transformer chamber and mixes with the low-temperature air. As a result, the temperature at the exhaust outlet is lower than that above the radiators. It can be seen in combination with Table 6 that areas with hot temperatures and high velocities correspond to each other. This is because higher air temperature and lower air density result in higher air velocity driven by the floating lift phenomenon. In Baseline Scheme 1 (Fig. 8 (a)), as analysed in section 5.1, the air temperature above the radiators closer to the inlet is lower, and the surface temperature of the radiators is also lower. In Scheme 2 (Fig. 8 (b)), it can be seen from Fig. 8 (d) that the surface temperature of the radiators gradually increases along the direction of airflow, and the surface temperature changes on both sides of the transformer are the same. This is because the air temperature is low, and the flow rate is high when the distance from the inlet is close. As the air volume decreases with distance from the inlet, the air temperature in contact with the radiator increases. In Scheme 3 (Fig. 8 (c)), due to the air inlet on both sides, the air inlet volume of the unilateral air inlet is halved. As shown in Fig. 8 (d), the radiator surface

Table 6
Velocity distribution of different cross-sections in the main transformer chamber under three different air inlet arrangement schemes.

Cross-section	Z = 0.5 m, Y = 2 m	Z = 0.5 m, Y = -2m
Baseline Scheme 1		
Scheme 2		
Scheme 3		

temperature in this air intake configuration is lower than that in Baseline Scheme 1. As the air volume of each inlet decreases, the surface temperature of radiators in groups 1–3, 9–11 is higher than that in Scheme 2. Compared to Baseline Scheme 1, both Scheme 2 and Scheme 3 result in lower surface temperatures of the radiators, and the temperature distribution on both sides of the transformer is more uniform.

In this paper, the energy utilization coefficient [36–39] is introduced to evaluate the ventilation and heat dissipation effects of indoor substations. The calculation formula is as follows:

$$\eta = \frac{T_{out} - T_{int}}{T_a - T_{int}} \tag{10}$$

where T_{int} is the inlet temperature, K; T_{out} is the outlet temperature, K; T_a is the average air temperature in the main transformer chamber, K. A larger energy utilization coefficient indicates better ventilation and heat dissipation performance.

Fig. 9 is a graphical representation that illustrates the impact of various positions of the air inlet on different parameters related to ventilation and heat dissipation in the indoor substation.

In Scheme 3, the air inlet of the main transformer chamber is positioned at the bottom of two opposite walls and is perpendicular to the plane where the radiators are located. This arrangement allows for efficient airflow organization, ensuring that the radiators receive an even distribution of cooling air and effectively utilize the cooling capacity of the air. As a result, the maximum temperature of the transformer is the lowest at 67.1 °C, indicating effective heat dissipation and the energy utilization coefficient is the highest at 0.96, indicating efficient utilization of energy. Therefore, Scheme 3 is considered the optimal design scheme for the ventilation and heat dissipation in the indoor substation.

The air inlet arrangement method in Scheme 3 can reduce the maximum temperature of the main transformer by 1.3 °C and increase the energy utilization coefficient by 9.1 % compared with that in Scheme 1. This indicates that the air inlet arrangement in Scheme 3 is more effective in cooling the transformer and utilizing energy efficiently than in Scheme 1.

The total inlet area of all three designs (Scheme 1, Scheme 2, and Scheme 3) is the same. However, due to the change in the inlet position, the mass flow rate of air entering the substation will vary slightly. In Scheme 3, the air volume is larger compared to the other

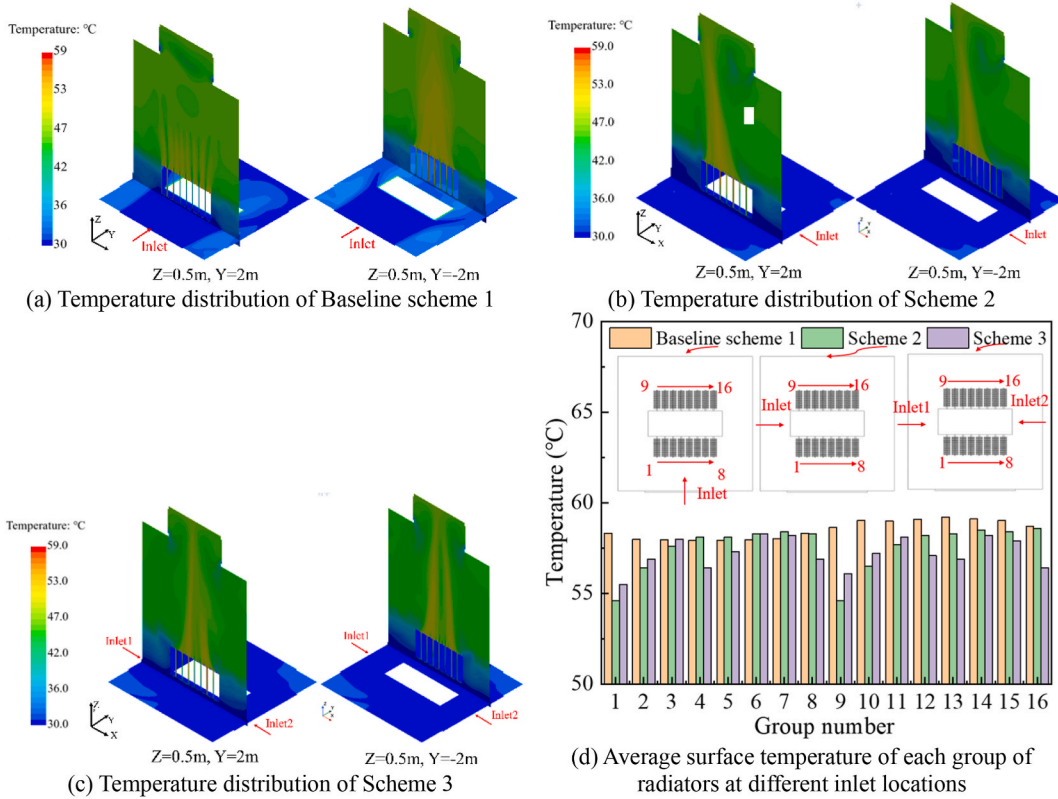


Fig. 8. Temperature distribution and average surface temperature of each group of radiators at different inlet locations.

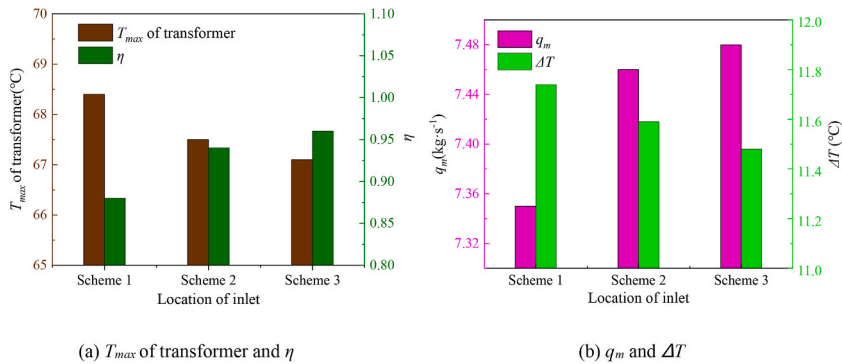


Fig. 9. The impact of different air inlet positions. (T_{max} of transformer—maximum temperature of the transformer, η – energy utilization coefficient, q_m – mass flow rate, ΔT – temperature difference of inlet and outlet).

designs, indicating that more air is entering the substation through the air inlet.

When the air inlet is positioned according to Scheme 3, it results in an increased thermal pressure difference between the indoor and outdoor environments. This means that there is a greater pressure difference driving the airflow inside the substation, facilitating better ventilation and heat dissipation. Additionally, the airflow resistance within the chamber is reduced, allowing for smoother airflow and improved ventilation performance. The variation in the temperature difference between the inlet and outlet is opposite to the variation in the air volume, and both are less than 15 °C, which meets the substation design specification [40].

5.2.2. The length of inlet and its impact on ventilation and heat dissipation

Taking the optimal inlet location model (Scheme 3) in 5.2.1 as the reference model, the influence of the inlet length on the ventilation and heat dissipation of the main transformer chamber is explored. In this paper, the length ratio is defined as the ratio of the length of the inlet (L) to the total width of the main transformer and radiators on both sides (L_r) (Fig. 10). The total area of the inlet is fixed at 6 m², and based on this, the length and height of the air inlet can be determined. Six different length ratio models are designed,

as shown in Table 7.

Fig. 11 shows the numerical simulation results provide information about the air distribution in the main transformer chamber with six different scenarios based on the length ratio of the air inlet.

When the length ratio is small (Fig. 11(e) and (f)), the length of the air inlet is shorter than the width of the radiators on both sides. This causes the air to be influenced by the transformer and deviate towards the outside of the radiators, creating a cooling air short circuit. As a result, the air entering the bottom of the radiators is reduced, which is not beneficial for heat dissipation. However, as the length ratio increases (Fig. 11(c) and (d)), the length of the air inlet becomes closer to the width of the radiators on both sides. This allows the air to cover the area where the radiators are located, resulting in even cooling of the radiators. Comparing Fig. 11(c) and (d), when the air inlet is slightly longer than the width of the radiators on both sides, the airflow deviation is minimal, and a larger amount of air flows into the radiators. Moreover, the flow rate above the radiators increases, facilitating the rapid discharge of warm air from the main transformer chamber. However, when the length of the air intake is significantly greater than the width of the radiators on both sides (Fig. 11(a) and (b)), some of the air does not flow into the bottom of the radiators but meets on the outside of the radiators. This creates eddy currents near the wall, reducing the utilization rate of the cooling wind.

Fig. 12 shows the temperature distribution of specific cross-sections in the main transformer chamber under different length ratios. As can be seen from Fig. 12, in the horizontal section, because of the formation of eddy currents at various positions, the air disturbance is enhanced. In the horizontal section of the transformer chamber, the airflow experiences turbulence due to the formation of eddy currents. Eddy currents are swirling motions of air caused by the interaction of different airflows. These eddy currents create disturbances in the airflow, leading to changes in the temperature distribution. The enhanced air disturbance caused by the eddy currents leads to a more effective mixing of hot and chilly air in the transformer chamber. This mixing results in an increase in the air temperature in the specific areas where the eddy currents are formed. However, because it is not near the radiators, it does not strengthen the heat dissipation of the radiators. Although the temperature rises in the areas affected by the eddy currents, these areas are not in close proximity to the radiators. The radiators are the components responsible for dissipating heat from the transformer. Therefore, the increased air temperature caused by the eddy currents does not directly contribute to the heat dissipation of the radiators. As the length ratio increases, the length of the air inlet becomes closer to the width of the radiators. This closer proximity allows the air to cover a larger area where the radiators are located. As a result, the radiators experience more effective cooling, leading to a decrease in the air temperature above them.

Fig. 13 is a graphical representation that illustrates the impact of the length ratio on various parameters related to heat dissipation in the main transformer chamber.

The graph shows that as the length ratio increases, the maximum temperature of the main transformer and the temperature difference between the inlet and outlet initially decrease and then increase. The energy utilization coefficient and mass flow rate initially increase and then decrease with an increase in the length ratio. The analysis reveals that when the length ratio is 1.10, which means the

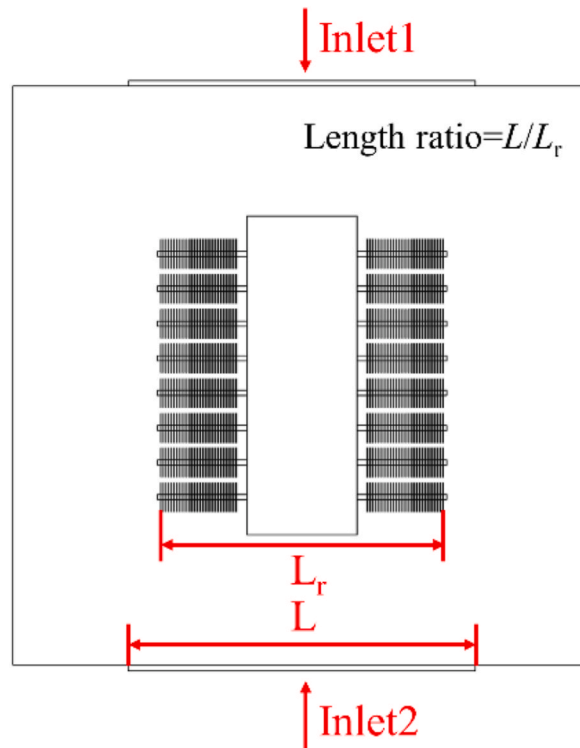


Fig. 10. The length of the inlet (L) and the total width of the main transformer and radiators on both sides (L_r).

Table 7
Length design schemes of the inlet.

Length ratio (L/L_r)	1.52	1.21	1.10	0.95	0.75	0.58
L (m)	7.50	6.00	5.45	4.68	3.60	2.88

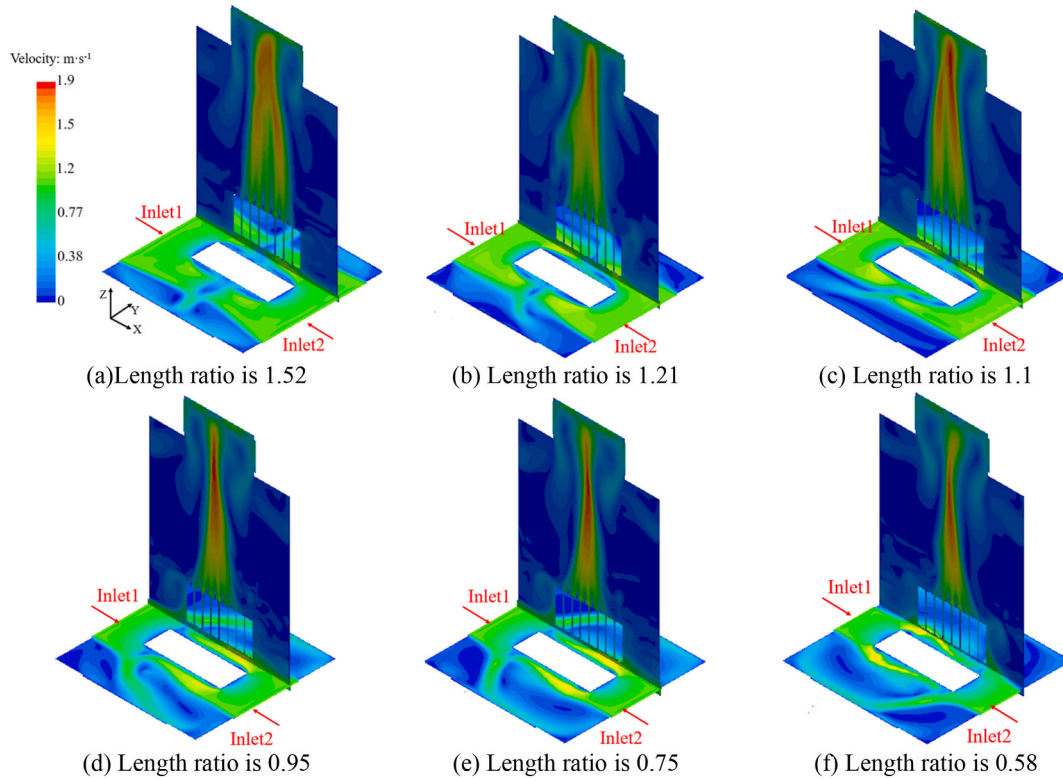


Fig. 11. Velocity distribution of specific cross sections in the main transformer at different length ratios.

length of the air inlet is 5.45 m and the height is 0.55 m, the main transformer chamber achieves the lowest maximum temperature of 67.4 °C. Additionally, this configuration results in the highest energy utilization coefficient of 0.969, indicating efficient heat dissipation. When compared to the reference model (Scheme 3), this optimal configuration reduces the maximum temperature by 0.4 °C and increases the energy utilization coefficient by 2.2 %.

The explanation highlights an important consideration when adjusting the length of the air inlet in the main transformer chamber. If the length of the inlet is reduced while the total ventilation area is kept unchanged, the height of the inlet needs to be increased to compensate. However, it is important to note that in this scenario, the change in length has a greater impact on the heat dissipation performance compared to the change in height.

5.2.3. The height of inlet and its impact on ventilation and heat dissipation

The model with a length ratio of 1.10 was used as the reference model, and the height of the air inlet was 0.55 m. In this paper, the height ratio is calculated by dividing the height of the air inlet by the height of the reference model. By varying the height ratio while keeping the length of the air inlet constant ($L = 5.45$ m), the effect of different air inlet heights on the ventilation and heat dissipation characteristics is studied. The air inlet height design schemes are shown in Table 8.

According to the numerical simulation results of the above model, the velocity distribution of the main transformer chamber is obtained as shown in Fig. 14. As can be seen from Fig. 14, because the length of the air inlet is unchanged, the area of the air inlet increases with an increase in the height of the air inlet. The simulation results indicate that as the height ratio increases, the wind speed at the inlet slightly increases, resulting in an increase in the total intake air volume. When the height ratio is small, the indoor air volume is also small, and the air in the main transformer chamber easily diffuses, leading to a less concentrated high-velocity area. However, as the height ratio increases, the high-velocity area becomes more concentrated. Additionally, when the indoor air volume is small, the warm air flowing to the exhaust outlet may not be enough to fill the entire outlet, causing chilly air from the outside to flow back into the main transformer chamber. This phenomenon becomes more pronounced as the height ratio decreases.

Fig. 15 shows the temperature distribution of specific cross-sections in the main transformer chamber under different height ratios. As can be seen from Fig. 15, with the increase in the height of the air inlet, the height of thermal stratification also increases. The air

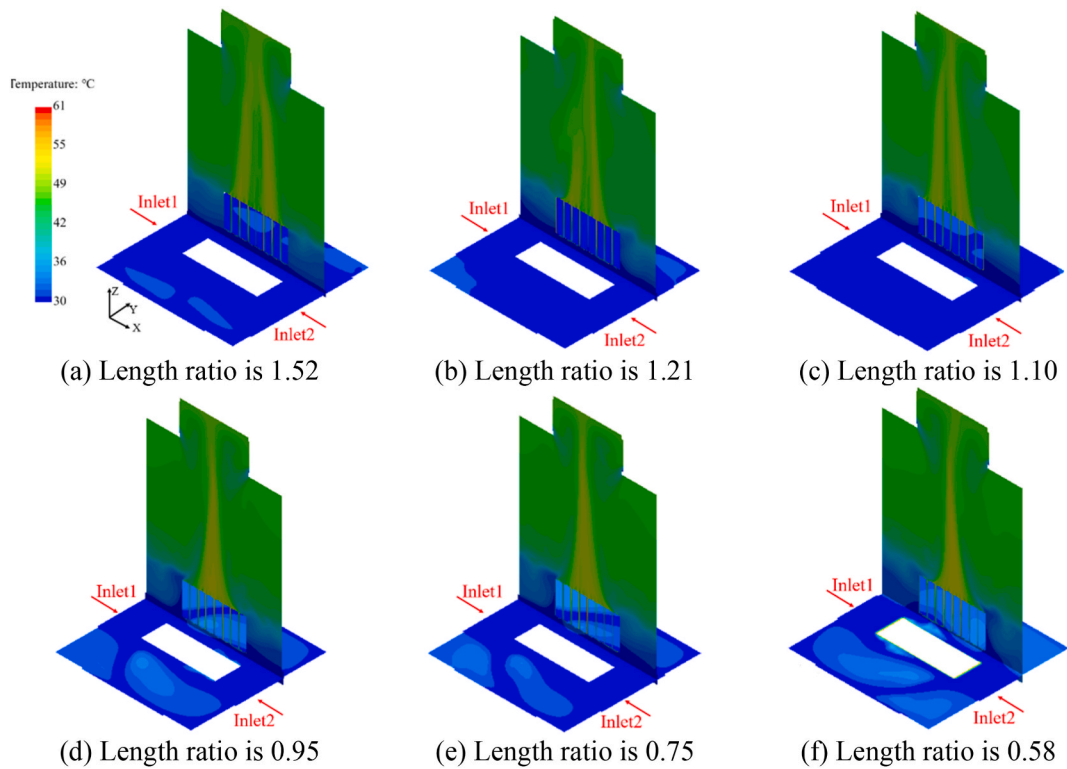


Fig. 12. Temperature distribution of specific cross sections in the main transformer at different length ratios.

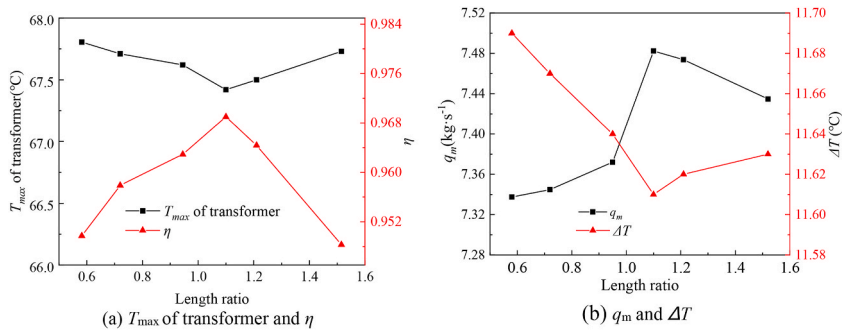


Fig. 13. The impact of different length ratios.

Table 8
Height design schemes of the inlet.

Height ratio ($H/0.55$)	1.0	0.9	0.8	0.7	0.6
H (m)	0.55	0.5	0.44	0.39	0.33

temperature above the radiators decreases. This is because the height of the inlet and the ventilation area increase, and the amount of air exchanging heat with the radiators increases, resulting in a decrease in the air temperature rise. Because the ambient temperature is lower than the indoor air temperature, the outside air density is high, and it will flow to the bottom of the main transformer chamber under the action of gravity. When the inlet air volume is small, the indoor warm air is not sufficient to occupy the entire exhaust outlet, resulting in the outdoor chilly air flowing into the chamber from the exhaust outlet. With an increase in the height ratio, the phenomenon of chilly air backflow is weakened.

Fig. 16 is a graphical representation that illustrates the relationship between the height ratio and various parameters in the study. In Fig. 16 (a), with an increase in the height ratio, the maximum temperature of the main transformer decreases, indicating better heat dissipation. Additionally, the energy utilization coefficient increases, suggesting that more energy is being effectively utilized in the

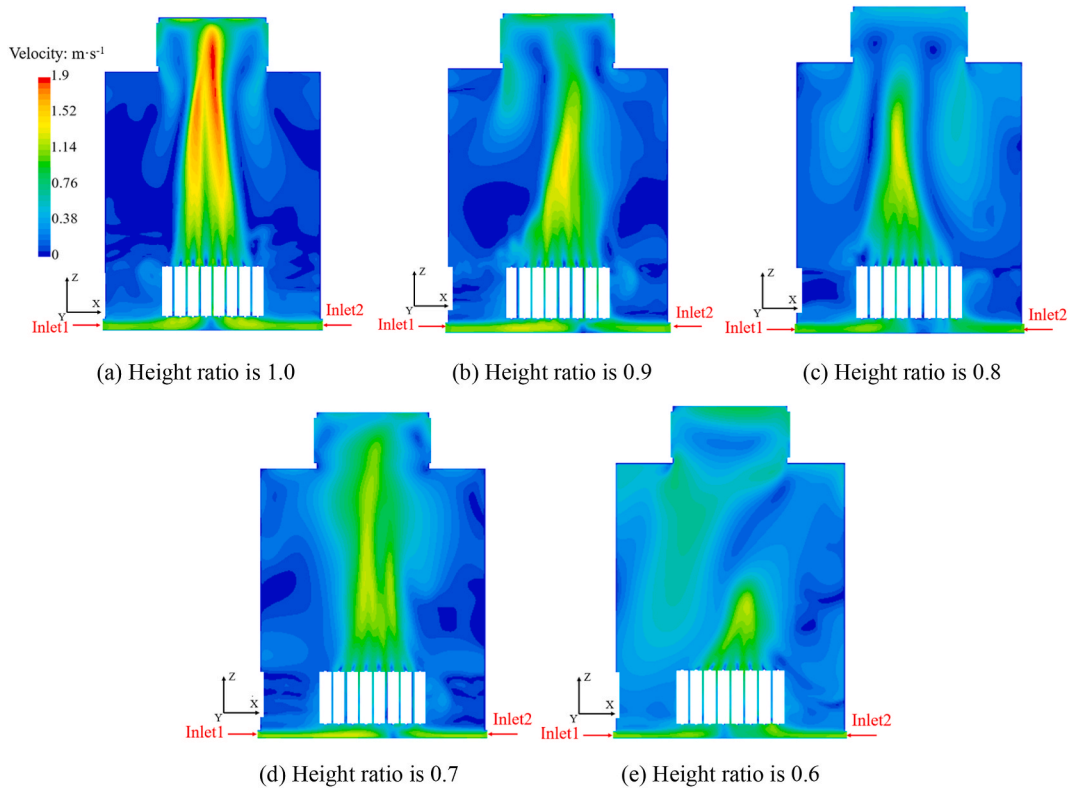


Fig. 14. Velocity distribution of specific cross sections in the main transformer at different height ratios.

system. In Fig. 16 (b), under the condition that the length of the inlet is fixed, demonstrated that as the height ratio increases, the resistance of external cooling air entering the main transformer chamber decreases. This implies that the airflow can enter the chamber more easily, leading to an increase in the air inlet volume of the main transformer chamber. The increase in air inlet volume allows for better ventilation and heat dissipation within the chamber. When the length ratio is greater than 0.8, the inlet and outlet temperature difference of the main transformer chamber is lower than $15\text{ }^{\circ}\text{C}$, which meets the ventilation and heat dissipation design specifications of the main transformer chamber [40].

In summary, the simulation results suggest that the height ratio of the air inlet plays a significant role in the ventilation and heat dissipation performance of the main transformer chamber. A smaller height ratio, indicating a lower height of the air inlet, leads to decreased air volume and energy utilization coefficient, as well as increased maximum temperature of the transformer and temperature difference between the inlet and outlet. On the other hand, a larger height ratio, indicating a higher height of the air inlet, results in a more concentrated high-velocity area and improved ventilation and heat dissipation performance.

5.3. The impact of the operating load

The study also examined the impact of the load rate of the transformer on ventilation and heat dissipation in the main transformer chamber. The load rate refers to the ratio of the actual load on the transformer to its rated load. The ambient temperature is maintained at $30\text{ }^{\circ}\text{C}$ during the study, and five different load rates are selected, each corresponding to a specific heating power (which can be calculated according to equation (9) and Table 4), as shown in Table 9.

Fig. 17 includes The of velocity distribution and the change of ventilation volume under different load rates in the main transformer chamber. The load rate is varied to observe its impact on the wind speed. The graph in Fig. 17 (a) shows that as the load rate, which refers to the amount of power being consumed by the transformer, increases, the wind speed within the main transformer chamber also increases. This means that as more power is being consumed by the transformer, more heat is being generated, resulting in a higher temperature difference between the indoor and outdoor areas. When the load rate of the transformer increases, it means that more power is being consumed, resulting in a higher heat output from the transformer. This increase in heat output leads to a larger temperature difference between the indoor and outdoor areas of the main transformer chamber. The larger temperature difference causes more air to be drawn into the chamber, resulting in an increase in the intake air volume. However, as can be seen from Fig. 17 (b) the relationship between the load rate and the intake air volume is not a simple linear relationship. This means that the increase in the intake air volume is not directly proportional to the increase in the load rate. Instead, the rate at which the intake air volume increases gradually decreases as the load rate increases. As the load rate of the transformer increases, the rate at which the intake air volume increases start to decrease. This means that the sensitivity of the air intake to the load rate decreases as the load rate becomes

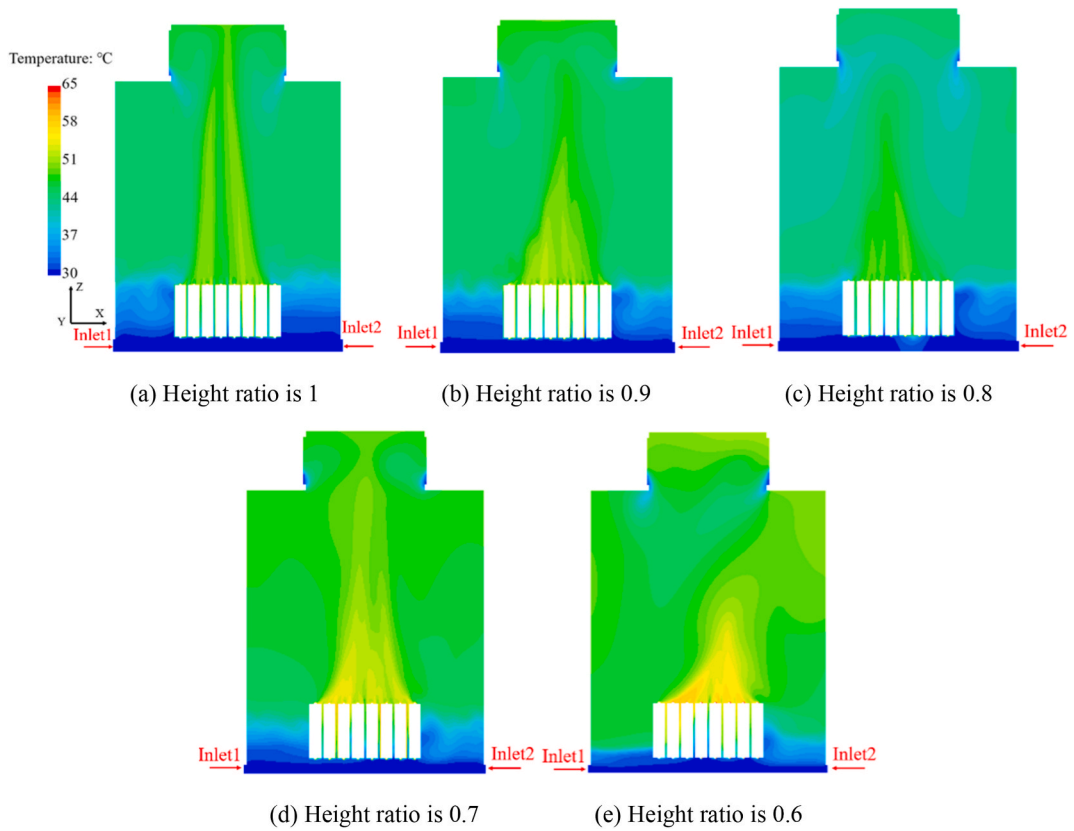


Fig. 15. Temperature distribution of specific cross sections in the main transformer at different height ratios.

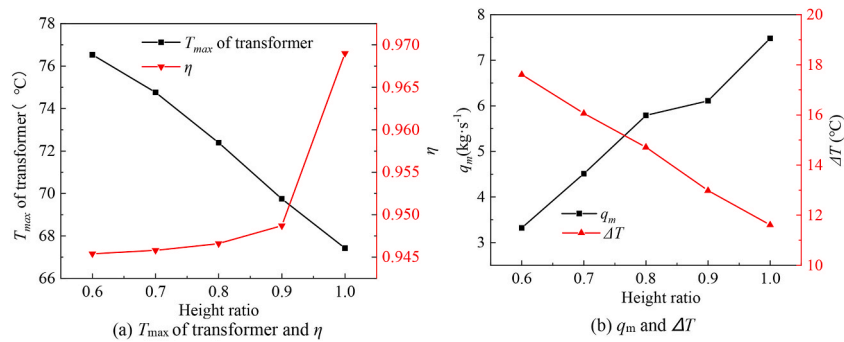


Fig. 16. The impact of different height ratios.

Table 9
Transformer heating power at different load rates.

Load rate	0.2	0.4	0.6	0.8	1
Heating power/kW	32.09	53.80	89.99	140.65	205.79

higher. In other words, when the load rate is already high, further increases in the load rate have a smaller impact on the intake air volume.

Figs. 18 and 19 are graphical representations that provide information about the temperature distribution and the influence of load rates on various parameters in the main transformer chamber of the indoor substation. As can be seen from Fig. 18, the temperature of the indoor air in the main transformer chamber increases as the load rate increases. This indicates that the heating power of the transformer also increases with the load rate, leading to higher air temperatures in the chamber. Even though the ventilation volume

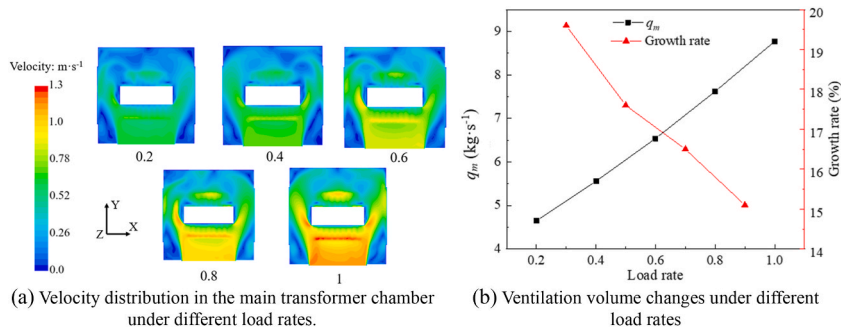


Fig. 17. The velocity distribution and the change of ventilation volume under different load rates.

increases with the load rate, the heating power of the transformer also increases simultaneously. This results in higher air temperatures in the main transformer chamber and causes the temperature of the main transformer to increase with the load rate. The load rate does not have a significant impact on how the air temperature changes with height in the main transformer chamber, as shown in Fig. 19 (b). However, as the load rate increases, the temperature gradient, or the rate at which the temperature changes with respect to height, increases below 3 m. As the load rate increases, the temperature difference between the inlet and outlet of the main transformer chamber also increases in Fig. 19 (a). This suggests that the increase in transformer heat due to the higher load rate is greater than the increase in the volume of air entering the chamber through the inlet. Note that in the case of a large load rate, the inlet and exhaust air temperature difference exceed 15 °C. In this case, this indicates that only relying on natural ventilation cannot meet indoor heat dissipation needs, and other cooling measures need to be taken in further research.

6. Conclusions

This numerical study aims to evaluate the efficacy of different air inlet designs and operating conditions on natural ventilation performance. The objectives are to analyse the impact of inlet location, dimensions, and transformer load on airflow distribution, temperature field, and cooling efficiency. Through this research, the following conclusions are obtained.

- (1) Compared to a single inlet configuration, staggered opposite inlets allow for a more even distribution of air on both sides of the transformer with no airflow attenuation. This configuration reduces the maximum transformer temperature by 1.3 °C and increase energy utilization by 9.1 %, indicating more effective heat removal.
- (2) Increasing the inlet length ratio, up to an optimal point, helps improve cooling. A length ratio of 1.1 led to a 0.4 °C lower maximum temperature and 2.2 % higher energy utilization versus the baseline design. The study reveals an optimal inlet length ratio of 1.1 that lowers transformer temperatures and increases energy utilization versus other ratios.
- (3) With the air inlet length unchanged, reducing inlet height was found to decrease airflow rates and cooling efficiency due to higher airflow resistance. Height ratios above 0.8 met the recommended design criteria for the substation ventilation system. With the increase of length ratio, the transformer temperature and energy utilization coefficient are increased.
- (4) The study also revealed limitations in relying solely on natural ventilation under high transformer load conditions. While intake air volumes increased with load, the rate of increase declined at higher loads. The inlet-outlet temperature difference exceeded 15 °C at high loads, indicating supplemental mechanical ventilation may be needed in these cases.

CRediT authorship contribution statement

Haomai Zhang: Writing – original draft, Visualization, Software. **Ling Wang:** Software. **Peng Yang:** Writing – review & editing. **Yingwen Liu:** Writing – review & editing, Project administration. **Chao Zhu:** Project administration. **Lv Wang:** Project administration. **Hua Zhong:** Writing – review & editing.

Declaration of Competing interest

We declare that we have no financial and personal relationships with other people or organizations that can inappropriately influence our work, there is no professional or other personal interest of any nature or kind in any product, service and/or company that

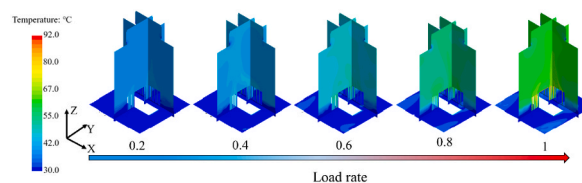


Fig. 18. Temperature distribution of different cross sections in the main transformer chamber under different load rates.

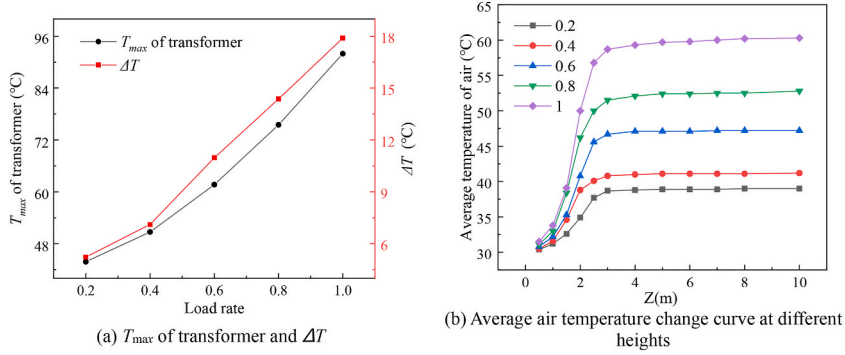


Fig. 19. The impact of different load rates.

could be construed as influencing the position presented in, or the review of, the manuscript entitled “Optimizing Air Inlet Designs for Enhanced Natural Ventilation in Indoor Substations: A Numerical Modelling and CFD Simulation Study”.

Data availability

Data will be made available on request.

Acknowledgements

The present work is supported by the National Natural Science Foundation of China (No. 52276019).

Nomenclature

symbols

Q	Heating power of the main transformer (kW)
P_0	No-load loss of the main transformer (kW)
β	Load rate of the main transformer
P_k	Load-loss of the main transformer (kW)
ρ	Density ($\text{kg}\cdot\text{m}^{-3}$)
\vec{u}_i	Velocity vector ($\text{m}\cdot\text{s}^{-1}$)
x_i	Directional component (m)
p	Pressure (Pa)
μ	Dynamic molecular viscosity ($\text{m}^2\cdot\text{s}^{-1}$)
μ_T	Turbulent eddy viscosity ($\text{m}^2\cdot\text{s}^{-1}$)
δ_{ij}	Kronecker delta
g_i	Acceleration of gravity ($\text{m}\cdot\text{s}^{-2}$)
c_p	Specific heat capacity ($\text{J}\cdot\text{kg}^{-1}\cdot\text{K}^{-1}$)
λ	Thermal molecular conductivity ($\text{W}\cdot\text{m}^{-1}\cdot\text{K}^{-1}$)
λ_T	Turbulent thermal conductivity ($\text{W}\cdot\text{m}^{-1}\cdot\text{K}^{-1}$)
T	Temperature (K)
$\nabla \cdot \vec{q}_r$	Radiation source term ($\text{W}\cdot\text{m}^{-2}$)
I_b	Blackbody intensity ($\text{W}\cdot\text{m}^{-3}$)
σ_a	Absorption coefficient
I	Radiation intensity ($\text{W}\cdot\text{m}^{-3}$)
\vec{r}	Position vector (m)
\vec{s}	Direction vector(m)
k	Turbulent kinetic energy ($\text{m}^2\cdot\text{s}^{-2}$)
ε	Turbulent kinetic energy dissipation rate ($\text{m}^2\cdot\text{s}^{-3}$)
I_λ	Radiation intensity at wavelength λ ($\text{W}\cdot\text{m}^{-3}$)
$I_{b\lambda}$	Blackbody intensity at wavelength λ ($\text{W}\cdot\text{m}^{-3}$)
$k_{a\lambda}$	Absorption coefficient
$k_{s\lambda}$	Scattering coefficient
$k_{pa\lambda}$	Particle absorption coefficient
$k_{ps\lambda}$	Particle scattering coefficient
s	Distance in the direction (m)

Ω	Solid angle (sr)
η	Energy utilization coefficient
q_m	Mass flow rate ($\text{kg}\cdot\text{s}^{-1}$)
ΔT	Temperature difference of inlet and outlet ($^{\circ}\text{C}$)

Abbreviations

out	Outlet of the main transformer chamber
int	Inlet of the main transformer chamber
a	Volume average
max	Maximum value

References

- [1] Tareq Saeed, Ibrahim Abbas, Finite element analyses of nonlinear DPL bioheat model in spherical tissues using experimental data, *Mech. Base. Des. Struct. Mach.* 50 (4) (2022) 1287–1297.
- [2] Marin Marin, Aatef Hobiny, Ibrahim Abbas, The effects of fractional time derivatives in porothermoelastic materials using finite element method, *Mathematics* 9 (14) (2021) 1606.
- [3] Aatef D. Hobinyand, Ibrahim A. Abbas, Nonlinear analysis of dual-phase lag bio-heat model in living tissues induced by laser irradiation, *J. Therm. Stresses* 43 (4) (2020) 503–511.
- [4] R. Xie, J. Huang, P. Zuo, F. Wang, Optimization of ventilation and heat dissipation structure of transformer chamber in Prefabricated substation based on multi-Physics coupling, in: 2023 IEEE 4th International Conference on Electrical Materials and Power Equipment (ICEMPE), 2023. Shanghai, China.
- [5] Yun Liu, Wenjie Ye, Yonghua Li, et al., Ventilation Optimization for reduction of indoor air temperature of main transformer chamber in urban indoor substation by the variational method, *J. Therm. Sci.* 28 (5) (2019).
- [6] M. Kanaan, K. Chahine, CFD study of ventilation for indoor multi-zone transformer substation, *International Journal of Heat and Technology* 36 (1) (2018) 88–94.
- [7] L.W. Xu, A.X. Zou, A fast computational fluid dynamics model for the flow and heat transfer characteristics analysis of indoor substation chambers, *IOP Conf. Ser. Mater. Sci. Eng.* 199 (1) (2017).
- [8] H. Liu, Y.P. Hao, M.L. Fu, et al., Study on ventilation of indoor substation main transformer chamber based on COMSOL software[C], in: International Conference on Electrical Materials and Power Equipment (ICEMPE), 2017, pp. 296–300. Xi'an, China.
- [9] H. Yang, T. Yu, X. Rui, et al., Numerical simulation of ventilation for main transformer chamber of indoor substations, *Open Autom. Control Syst. J.* 7 (1) (2015) 630–639.
- [10] L. Cheng, H. Wen, J. Zhang, C. Liu, J. Hao, W. Li, Influence of box-in structure on heat dissipation performance of UHV Converter transformer, in: 2021 IEEE 4th International Electrical and Energy Conference (CIEEC), 2021. Wuhan, China.
- [11] C. Wei, H. Sheng, T. Qi, X. Yin'e, Optimization of ventilation and heat dispersion for split type of indoor transformer, in: 2021 IEEE International Conference on Advances in Electrical Engineering and Computer Applications (AEECA), 2021. Dalian, China.
- [12] W. Bengang, H. Hua, L. Honglei, et al., Study on simulation test device of transformer split type cooling system, *Energy Proc.* 100 (2016) 556–560.
- [13] C. Ramos, M. Beiza, J. Gastelurrutia, et al., Numerical modelling of the natural ventilation of underground transformer substations, *Appl. Therm. Eng.* 51 (1) (2013) 852–863.
- [14] Bidarmaghz Asal, Makasis Nikolas, Fei Wenbin, et al., An efficient and sustainable approach for cooling underground substations, *Tunnelling and Underground Space Technology incorporating Trenchless Technology Research* (2021) 113.
- [15] Ying Wang, Xu Jin, Jiapeng Zhang, et al., Scheme design and energy-saving Optimization of Cold and heat energy supply system for substation main Control building in Cold area, *Appl. Sci.* 14 (4) (2024) 1562.
- [16] S. Wiriyasart, P. Naphon, Numerical study on air ventilation in the workshop chamber with multiple heat sources, *Case Stud. Therm. Eng.* 13 (2019) 100405.
- [17] Chenxiao Zheng, Shijun You, Huan Zhang, et al., Comparison of air-conditioning systems with bottom-supply and side-supply modes in a typical office chamber, *Appl. Energy* (2018) 227.
- [18] S.J. Mei, J.T. Hu, L. Di, et al., Thermal buoyancy driven flows inside the industrial buildings primarily ventilated by the mechanical fans: local facilitation and infiltration, *Energy Build.* 175 (2018) 87–101.
- [19] Adryan Seng Theng Ang, et al., Natural ventilation and indoor air quality in Domestic School building: CFD simulation and Improvement Strategies, *CFD Lett.* 16 (3) (2024) 1–14.
- [20] Shuaikun Yue, et al., Analysis of the ventilation performance of a solar Chimney coupled to an outdoor wind and indoor heat source, *Appl. Sci.* 13 (4) (2023) 2585.
- [21] Changqing Yang, Wenhao Luo, Angui Li, et al., Natural ventilation driven by a restricted heat source elevated to different levels, *Build. Simulat.* 15 (2) (2021).
- [22] Tao Yao, Haihua Zhang, Lili Zhang, et al., Ventilation performance of a naturally ventilated double-skin facade in buildings, *Renew. Energy* (2020) (prepublish).
- [23] Huai Chen, et al., An experimental case study of natural ventilation effects on the residential thermal environment and predicted thermal comfort in Kunming, *Case Stud. Therm. Eng.* (2024) 104198.
- [24] Chalermwat Tantasavasdi, Senatanit Arttamart, Natthaumporn Inprom, Combined wind catchers and side windows for cross ventilation in row houses, *J. Eng. Des. Technol.* (2024).
- [25] Yongcai Li, et al., Combining use of natural ventilation, external shading, cool roof and thermal mass to improve indoor thermal environment: field measurements and simulation study, *J. Build. Eng.* (2024) 108904.
- [26] Rachid Hidki, et al., Analysis of mixed convection and surface radiation in a horizontal channel containing different finned heat-generating blocks, *Therm. Sci. Eng. Prog.* 48 (2024) 102370.
- [27] Mohammad Foruzan Nia, Amir Babak Ansari, Seyyed Abdolreza Gandjalikhan Nassab, Transient combined volumetric radiation and free convection in a chamber with a hollow heat-generating solid body, *Int. Commun. Heat Mass Tran.* 119 (2020) 104937.
- [28] Rachid Hidki, et al., Natural convection coupled to surface radiation in an air-filled square cavity containing two heat-generating bodies, *Heat Transfer* 52 (3) (2023) 2143–2164.
- [29] D. Hao, Z. Chao, L. Yingwen, Thermal performance of double-layer porous-microchannel with phase change slurry, *Appl. Therm. Eng.* (2022) 211.
- [30] P.H. Oosthuizen, D. Naylor, An Introduction to Convective Heat Transfer Analysis, McGraw-Hill, 1999.
- [31] B.E. Launder, D.B. Spalding, Mathematical Models of Turbulence, Academic Press, 1973.
- [32] STAR-CCM+2206, Tutorials of the STAR-CCM+2206, SIEMENS, 2022.
- [33] César Porras-Amores, et al., Natural ventilation analysis in an underground construction: CFD simulation and experimental validation, *Tunn. Undergr. Space Technol.* 90 (2019) 162–173.
- [34] S. Jafari, V. Kalantar, Numerical simulation of natural ventilation with passive cooling by diagonal solar chimneys and windcatcher and water spray system in a hot and dry climate, *Energy Build.* 256 (2022) 111714.

- [35] Yu Chen, Xu Zhihao, et al., The study about CFD Algorithms of natural ventilation, *Refrig. Air Cond.* 25 (2019) 78–81.
- [36] S. Panchal, K. Gudlanarva, M.K. Tran, et al., Numerical simulation of cooling plate using K-epsilon turbulence model to cool down large-sized graphite/LiFePO4 battery at high C-rates, *World Electric Vehicle Journal* 13 (8) (2022) 138.
- [37] Li Han, Zheng Fu, Xi Chang, et al., Study on the impact of parallel jet spacing on the performance of multi-jet stratum ventilation, *Appl. Energy* 306 (2022).
- [38] T. Karimipannah, H.B. Awbi, M. Sandberg, C. Blomqvist, Investigation of air quality, comfort parameters and effectiveness for two floor-level air supply systems in classchambers, *Build. Environ.* 42 (2) (2007).
- [39] R. Gao, H. Zhang, A. Li, et al., A new evaluation indicator of air distribution in buildings, *Sustain. Cities Soc.* 53 (2020) 101836.
- [40] Ministry of Housing and Urban-Rural Development of the people's Republic of China, Code for Design of 35kV-110kV Substation (GB50059-2011), 2012 (in Chinese).